Int. J. Electrochem. Sci., 16 **(2021)** Article ID: 210352, doi: 10.20964/2021.03.18

International Journal of
ELECTROCHEMICAL
SCIENCE
www.electrochemsci.org

Cerium Doped Trimethoxy Silane-Aluminium Isopropoxide Coatings for Enhanced Corrosion Protection of 1061 Aluminum Alloy in Aqueous Sodium Chloride Solution

Wei Liu, Chengqiang An[*]*, Jianjun Hao, Wenruo Li*

School of Environmental and Chemical Engineering, Shenyang Ligong University, Shengyang, 110159, P R China
[*]E-mail: 1031757850@qq.com

Received: 2 October 2020 / *Accepted:* 18 December 2020 / *Published:* 31 January 2021

Aluminum alloy is the most widely used light metal material in recent years, and the corrosion resistance of aluminum alloy is currently a research hotspot in the field of materials. In this work, the purpose of using $Ce(NO_3)_3$ doped trimethoxy silane-aluminium isopropoxide (GPTMS-AIP) coating is to improve the corrosion resistance of aluminum alloy. SEM, EDS and Fourier transform infrared spectroscopy(FT-IR) were used to analyze the microscopic morphology and composition of the coating, and the potentiodynamic polarization measurements and electrochemical impedance method were used to investigate the influence of the content on the corrosion resistance of the coating and the corrosion behavior of the coating. The results showed that when the addition amount of $Ce(NO_3)_3$ was 0.5 g/L, the coating was homogeneous and flat with fewer defects. The corrosion behavior analysis proves that Ce^{3+} in the coating is released to generate $Ce(OH)_3$ and CeO_2, which can repair the coating and make coating have a certain self-repairing effect.

Keywords: corrosion resistance, self-repairing, composite coating, rare-earth salts

1. INTRODUCTION

Aluminum is the highest-content metal in the earth's crust and the second most used metal in the world only behind iron and steel[1]. It is widely used in industries and daily life due to its light weight, good machining performance, excellent electrical and thermal conductivity, high strength-to-weight ratio and oxidation resistance[2]. In recent years, in order to improve the maneuverability and operating speed of transportation vehicles to adapt to the rapid development of high-speed rail trains, automobiles, navigation and other transportation industries, the most feasible way is to reduce structural weight. Therefore, a large number of high-performance aluminum alloy components with low-density and high-strength have been used worldwide. For example, aluminum has gradually

replaced steel in the application of modern aerospace materials for several years and it can be an irreplaceable material for a long time.

Aluminum and its alloys can be passivated in the atmosphere to form a dense oxide coating on its surface, which can reduce the corrosion rate and improve the corrosion resistance of the substrate. However, this passivation coating is easily damaged by corrosive anions in corrosive environment, especially chloride ions, which cause the substation to be corroded. The most common corrosion forms of aluminum alloys are: pitting corrosion, galvanic corrosion, filiform corrosion, layered corrosion, intergranular corrosion, stress corrosion[3-6].

Chromating is one of the most used surface treatment technologies with the best corrosion resistance in industrial production. The metal surface after chromating treatment will form a high corrosion resistant passive coating with self-healing function, which has a good protective effect on the metal surface[7-9]. Despite all the advantages of chromate conversion coating, there is also a very serious problem: chromium in coating is mainly in the form of Cr^{6+} and Cr^{3+}. Cr^{6+} is known to be toxic and can cause great harm to the environment and threaten people's health. Therefore, many enterprises have developed low-toxic, environmentally friendly chromium-free passivation process to replace the use of chromate, so as to ensure people's health and achieve sustainable environmental development[10]. Many experts and scholars have done a lot of research on the chrome-free passivation treatment of aluminum alloy surface[11-14], among which inorganic-organic compound passivation has attracted wide attention[15-16]. Organic passivation and inorganic passivation are used in combination, which enables complementary properties and co-corrosion inhibition between inorganic and organic molecules, strengthens the protective effect of the coating on metals, and compensates for the performance defects of a single passivation coating.

C.A. Hernandez-Barrios[17] added an appropriate proportion of $Ce(NO_3)_3$ to the TEOS and GPTMS mixtures to prepare a continuous and uniform composite coating with good corrosion resistance, and the addition of $Ce(NO_3)_3$ reduced pH of the solution as well as accelerated the gel dynamics process of silane solution. Palomino[19] added Ce and nano-SiO_2 particles into silane solution, which proved the synergistic effect between them. Moreover, Ce and silane cross-linked in the process of coating formation, which greatly improved silicon content in the coating. Cabral[20] used scanning vibration electrode technology (SVET) and electrochemical AC impedance (EIS) to study the self-healing properties of $Ce(NO_3)_3$ doped silane coating. The test results showed that the silicone coating doped with $Ce(NO_3)_3$ had a significant reduction in current density after soaking 24 h, while current density at the defect of the non-doped silane coating increased significantly, and also proved that the addition of rare earths salts made the coating have good self-healing properties. M.F. Ontemoret[21] respectively added $La(NO_3)_3$ and $Ce(NO_3)_3$ to BTSE and BTSPS solutions. It was found that the coating adhesion and corrosion resistance were significantly improved by 2 orders of magnitude. At the same time, V.Palanivel[15] found that cerium nitrate as an inorganic corrosion inhibitor, can give silane coatings self-healing properties similar to the chromium passivation coatings.

On this basis, the purpose of this study was to evaluate the influence of doped $Ce(NO_3)_3$ on the anticorrosion features of GPTMS-AIP coating coated on aluminum alloy and its corrosion behavior.

2. EXPERIMENT

2.1. Material

The metallic substrate employed was 1060 aluminum alloy, cut to specimens with dimensions of 35 mm×35 mm×1 mm. The main chemical composition of 1060 aluminum alloy is shown in Table 1.

Table 1. Elemental Composition of 1060 aluminum alloy

Components	Al	Fe	Si	Cu	Zn	V	Ti	Mn	Mg
wt%	99.6	0.35	0.25	0.05	0.05	0.05	0.03	0.03	0.03

2.2. Preparation of GPTMS-AIP-Ce(NO$_3$)$_3$ coating

Aluminum alloy samples need to go through a pre-treatment process before coating. The aluminum metal surface was polished with different grades of emery paper (#400, #800, #1200) until the surface became smooth and shiny. The polished samples were caustic washed in the alkaline solution at 80 ℃ for 30 s (the composition of alkaline solution is 40 g/L Na_2CO_3, 30g/L $NaPO_4 \cdot 12H_2O$, 10g/L $NaSiO_3 \cdot 9H_2O$) to remove oil stains from the surface and then rinsed with double distilled water and dried in air stream.

The solution was prepared by mixing 2g trimethoxy silane (GPTMS) and 17g distilled water in a beaker, stirring at room temperature, and then adding 1g anhydrous ethanol slowly into the beaker. After stirring for 15 minutes, 1g aluminum isopropoxide (AIP) and concentration of 0.1 g/L-1 g/L $Ce(NO_3)_3$ were slowly added into the above solution in batches and continued stirring for 10 hours. Finally, stand the solution for 12 hours and take the supernatant in a beaker for later use.

Homogeneous and transparent coating was prepared on aluminum substrates by dip coating technique. Then the coated aluminum substrates were dried in a hot air oven at 200 ℃ for 15 min.

2.3. Characterization of GPTMS-AIP-Ce(NO$_3$)$_3$ Coating

All electrochemical experiments were carried out on the electrochemical workstation(CHI660E). A three-electrode system was used to test the corrosion performance of the coating in 3.5% NaCl solution. The sample was the working electrode, the saturated calomel electrode (SCE) was the reference electrode and the platinum electrode was the counter electrode. The tests were carried out at room temperature, the test area was 1cm^2. In the potentiodynamic polarization measurements, the sine wave excitation signal was 5mA, and the scanning speed of the polarization curve was 0.005 V/s. In the electrochemical impedance spectroscopy test, the initial potential was the open circuit potential, and the frequency range was 0.01 Hz-100000 Hz. The open circuit potential

(OCP) and electrochemical impedance spectroscopy (EIS) were used to test samples with different immersion time in 5.0 wt% NaCl solution, in order to analyze the corrosion behavior of samples.

The Fourier transform infrared spectroscopy (FT-IR, Bruker Vertex70v) was used to analyze the structure of the solution and GPTMS-AIP-Ce$(NO_3)_3$ coatings, and the scanning range was 400-4000 cm^{-1}. The scanning electron microscope(SEM, VEGA3 XMV) and energy dispersive spectroscope (EDS) were used to observe the microscopic morphology and element composition of the coatings.

3. RESULTS AND DISCUSSION

3.1 Effect of Ce$(NO_3)_3$ on the microstructure and composition of the coating

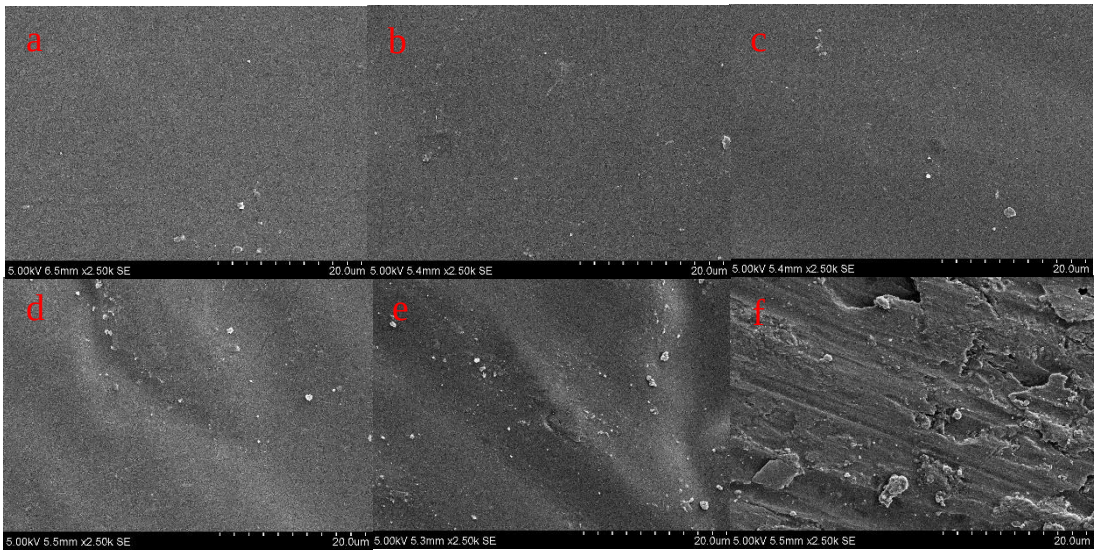

Figure 1. SEM diagram of GPTMS-AIP-Ce$(NO_3)_3$ coatings a. GPTMS-AIP-0 b. GPTMS-AIP-0.1 c. GPTMS-AIP-0.3 d. GPTMS-AIP-0.5 e. GPTMS-AIP-0.7 f. GPTMS-AIP-1.0

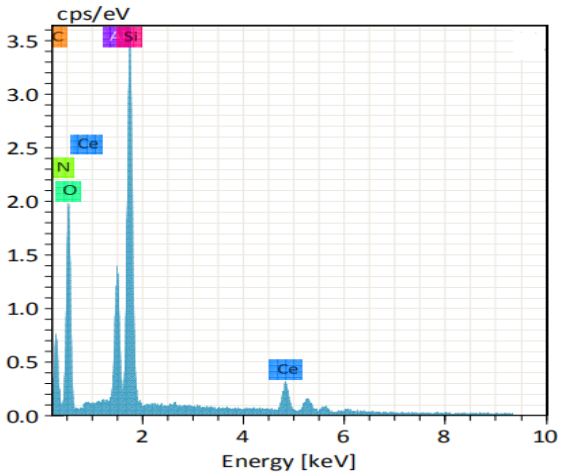

Figure 2. EDS diagram of GPTMS-AIP-0.3 coating

Fig. 1 shows the SEM diagram of GPTMS-AIP coating doped with different addition of $Ce(NO_3)_3$. Compared with GPTMS-AIP coating, the number of white particles attached to GPTMS-AIP-$Ce(NO_3)_3$ coating has increased because of incompletely reacted $Ce(NO_3)_3$ particles adhere to the surface of coating. In addition, roughness of the coating doped with $Ce(NO_3)_3$ is obviously increased. When the concentration is low, the surface of the coating is homogeneous and flat. However, wrinkles and defects appear on the surface of coating when the concentration is high. The same result was obtained in Pan's study[22], which proved that $Ce(NO_3)_3$ is an inorganic salt with catalytic action, which can enhance the reaction of conversion coating and lead to loose and uneven coating. Fig.2 shows the EDS diagram of GPTMS-AIP-0.3 coating. It can be clearly seen that there are C, O, N, Al, Si and Ce elements in the coating.

3.2 FT-IR studies

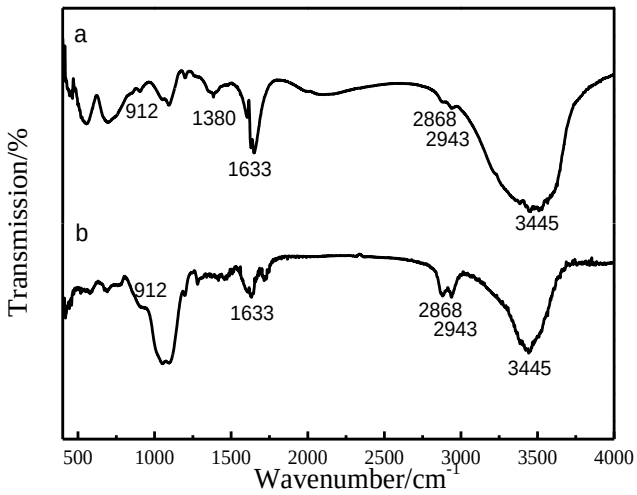

Figure 3. Fourier infrared spectrogram of GPTMS-AIP-0.3 system (a.solution b.coating)

Fig. 3 shows the FT-IR spectra of the GPTMS-AIP-0.3 solution/coating on the aluminum alloy surface. It can be clearly seen that the peak at 3445 cm^{-1} is caused by the stretching vibration of -OH, the peaks at 2868 cm^{-1} and 2943 cm^{-1} are caused by the stretching vibration of -CH, and 1633 cm^{-1} is the vibration of Si-OH. The above functional groups are all characteristic peaks of GPTMS and AIP. In addition, peaks appear at both 1147 cm^{-1} and 1100 cm^{-1} in Fig.3(a) and Fig.3(b). These peaks are caused by the Si-O-Si band produced by the condensation reaction. The peak at 912 cm^{-1} in Fig.1(a) accounting for Al-O-Si bond formation confirmed the hydrolysis and condensation reaction between AIP and GPTMS[17]. In addition, Ce^{3+} presence within the solution is confirmed through the band situated at 1380 cm^{-1} that is originated by the asymmetric stretching of the nitrate ion (NO_3^-), which comes from the dissociation of the $Ce(NO_3)_3$[18].

3.3 Corrosion evaluation of GPTMS-AIP-Ce(NO$_3$)$_3$ Coating

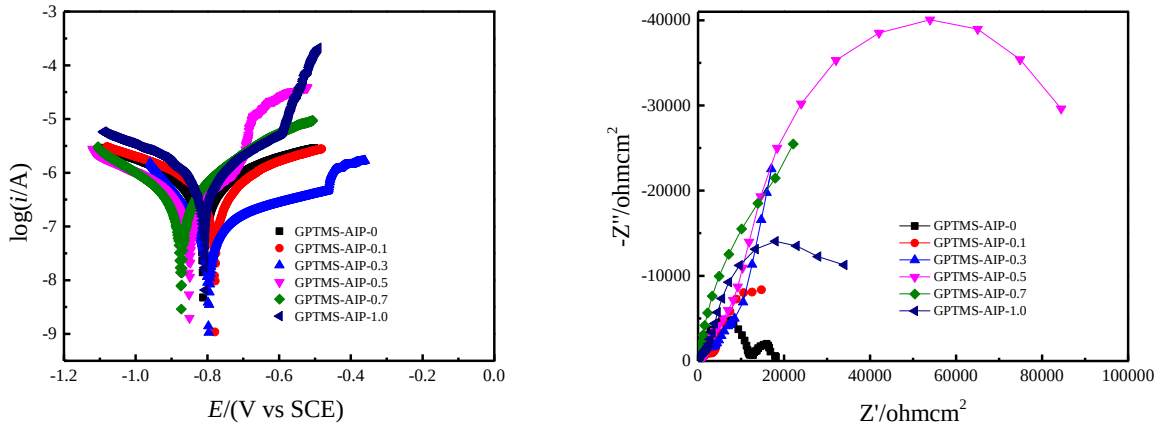

Figure 4. Potentiodynamic polarization curves and Nyquist plots of GPTMS-AIP-Ce(NO$_3$)$_3$ coatings in 3.5% NaCl. a. potentiodynamic polarization curves. b. electrochemical impedance.

The polarization curve is an electrochemical test method used to evaluate corrosion resistance of coatings and materials. Corrosion potential represents the corrosion tendency of the coating. The more positive the potential, the lower the corrosion tendency of coating and the better its corrosion resistance is. Fig. 4(a) shows the potentiodynamic polarization curves of GPTMS-AIP-Ce(NO$_3$)$_3$ coatings with different Ce^{3+} concentration. According to the fig.4, with the increase of Ce(NO$_3$)$_3$ concentration, the corrosion potential did not change significantly, which indicated that the addition of Ce(NO$_3$)$_3$ did not reduce the corrosion tendency of the coating. However, compared to the corrosion potential, corrosion current can evaluate the corrosion rate of the coating, which is a more important corrosion evaluation standard. Table 2 shows the fitting results of potentiodynamic polarization curve of GPTMS-AIP-Ce(NO$_3$)$_3$ coatings with different Ce^{3+} concentration. The calculation formula is Stern-Geary equation [23]:

$$R_p = \frac{b_a b_c}{2.303 i_{corr}(b_a + b_c)}$$

R_p—Polarization resistance, Ω

I_{corr}—The value of corrosion current density corresponding to the intersection of cathodic polarization curve and anodic polarization curve tangent, A • cm^{-2}

b_a—Tafel slope of cathode polarization curve

b_c—Tafel slope of anodic polarization curve

η is the corrosion inhibition efficiency, and its calculation formula is:

$$\eta = \frac{i_0 - i_{corr}}{i_0}$$

According to the table, coating corrosion current decreased by an order of magnitude after doping cerium nitrate, indicating that the addition of cerium nitrate can effectively reduce the corrosion rate of aluminum alloy, greatly improving the corrosion resistance of the substrate. Furthermore, with the increase of Ce(NO$_3$)$_3$ concentration, corrosion current rise after falling first. When the Ce(NO$_3$)$_3$

concentration is 0.5 g/L, corrosion current is the smallest, 1.35×10^{-7} A·cm^{-2}, polarization resistance is 5.71×10^{6} Ω·cm^{2}, corrosion inhibition efficiency reached 89.29%.

Electrochemical impedance spectroscopy is a non-destructive testing method. The protection mechanism and corrosion resistance principle of GPTMS-AIP-Ce$(NO_3)_3$ are studied by the electrochemical impedance method. 3.5% NaCl solution was prepared as corrosion medium. Fig.4(b) shows Nyquist plots of GPTMS-AIP-Ce$(NO_3)_3$ coatings with different Ce^{3+} concentration. The curve is composed of a small capacitive reactance arc in the high frequency region and large capacitive reactance arc in the low frequency region, which is a typical multilayer structure characteristic. The radius of the capacitive reactance arc represents the resistance of the coating. The larger the radius is, the stronger the blocking effect of the coating is, which hinders the entry of the corrosive solution and can play a good role in protecting the substrate.

Table 2. Potentiodynamic polarization curve data of GPTMS-AIP-Ce$(NO_3)_3$ coatings in 3.5% NaCl

Sample	i_{corr}/ (A·cm^{-2})	E_{corr}(V)	Rp/(Ω·cm^{2})	η
GPTMS-AIP-0	1.26×10^{-6}	-0.812	6105989.5	-
GPTMS-AIP-0.1	7.9×10^{-7}	-0.779	823545.15	37.30%
GPTMS-AIP-0.3	3.16×10^{-7}	-0.796	3221082.66	74.92%
GPTMS-AIP-0.5	1.35×10^{-7}	-0.849	5712612.32	89.29%
GPTMS-AIP-0.7	1.98×10^{-7}	-0.875	4052138.55	84.29%
GPTMS-AIP-1	6.6×10^{-7}	-0.807	885267.07	47.62%

Fig. 5 shows bode plots of GPTMS-AIP-Ce$(NO_3)_3$ coatings with different Ce^{3+} concentration. The impedance value of low measured frequency is usually used to evaluate the corrosion resistance of the coating. The higher the impedance, the more difficult it is for electrolyte solution to diffuse in the coating. According to the Bode-phase curve, coatings doped with Ce$(NO_3)_3$ have better corrosion resistance, and coating's impedance increases by nearly an order of magnitude. Moreover, the bode phase diagram of the doped coating shows an additional time constant, which is related to the coating of Ce^{3+}. Lower phase peak is usually associated with component defects such as pores and cracks in the coating. Combined with SEM diagram(Fig.1), the doping of Ce$(NO_3)_3$ increased the roughness of the coating and caused defects at high concentration, which made its phase peak lower than the coating undoped.

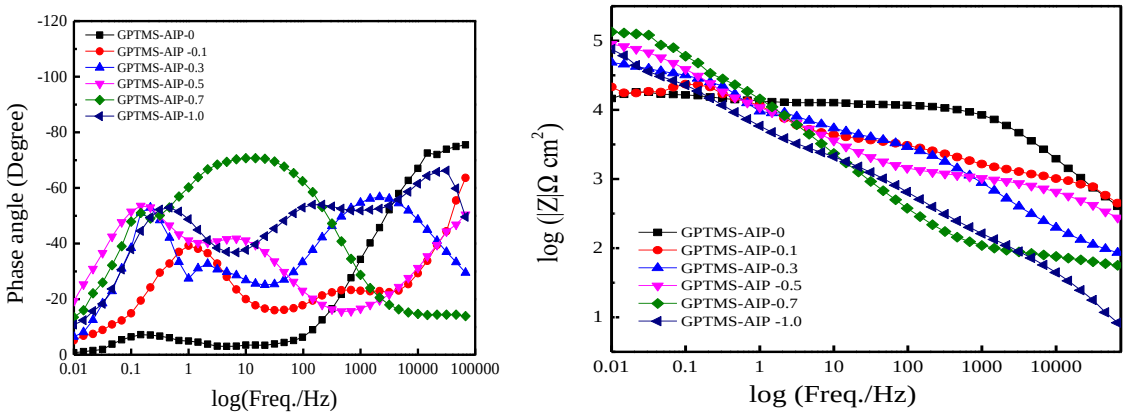

Figure 5. Bode plots of GPTMS-AIP-$Ce(NO_3)_3$ coatings in 3.5% NaCl.

In order to evaluate the corrosion resistance of the coating more accurately, EIS data can be fitted through an equivalent circuit. The coating is not a pure capacitor in the actual system and constant phase Angle element (CPE) is always used to replace the pure capacitor (C) in the fitting process, which can better reflect the real situation of the system. The impedance value of CPE can be calculated by the following formula:

$$Z_{CPE} = \frac{1}{Y_0} \bullet (j\omega)^{-n}$$

Y_0 is the modulus of CPE, its dimension is $\Omega^{-1} \cdot cm^{-2} \cdot s^{-n}$, j is the imaginary part parameter, ω is the angular frequency and n is the dispersion index, its value range is $0<n\leq1$. When n=1, CPE represents pure capacitance.

The equivalent circuit used to fit the impedance spectra is shown in Figure 6, and (a) is the equivalent circuit of the GPTMS-AIP coating, (b) is the equivalent circuit of the GPTMS-AIP - $Ce(NO_3)_3$ coating. Rs, Rpo, Rdl and Rox are respectively solution resistance, coating resistance, charge transfer resistance and Ce^{3+} doped layer resistance in the electrode process. CPE_C, CPEox and CPEdl are the coating capacitance, Ce^{3+} doped layer capacitance and electric double-layer capacitance between the electrode and the electrolyte, respectively. The data is shown in Table 3. It can be clearly seen that the coating has the best corrosion resistance when the concentration of $Ce(NO_3)_3$ is 0.5 g/L.

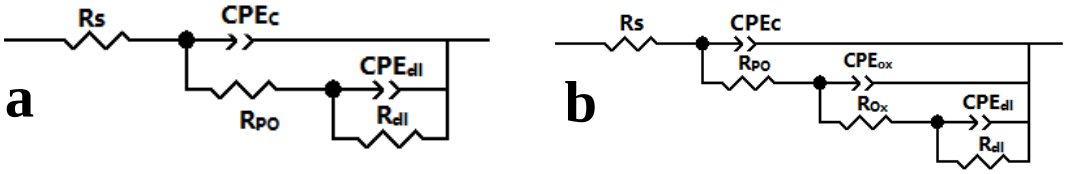

Figure 6. equivalent circuit of GPTMS-AIP-$Ce(NO_3)_3$ coating a.0g/L. b.0.1~1g/L.

Table 3. Electrochemical impedance parameters of GPTMS-AIP-Ce$(NO_3)_3$ coatings .

Sample	R_{PO} ($\Omega\cdot cm^2$)	CPE_C		R_{OX} ($\Omega\cdot cm^2$)	CPEox		Rct ($\Omega\cdot cm^2$)	CPEdl	
		Y_0 ($F\cdot cm^{-2}$)	n		Y_0 ($F\cdot cm^{-2}$)	n		Y_0 ($F\cdot cm^{-2}$)	n
GPTMS-AIP-0	12243	5.2×10^{-8}	0.82	-	-	-	6422	1.4×10^{-4}	0.66
GPTMS-AIP-0.1	4967	1.2×10^{-5}	0.46	14245	1.2×10^{-5}	0.95	10970	3.8×10^{-5}	0.34
GPTMS-AIP-0.3	4398	1.6×10^{-6}	0.74	15245	3.8×10^{-5}	0.58	35273	3.4×10^{-5}	0.65
GPTMS-AIP-0.5	1006	8.1×10^{-7}	0.69	14245	1.7×10^{-5}	0.73	90970	2.7×10^{-5}	0.92
GPTMS-AIP-0.7	9500	7.8×10^{-6}	0.9	24000	3.8×10^{-6}	0.8	68000	1.6×10^{-5}	0.99
GPTMS-AIP-1	3730	4.3×10^{-5}	0.56	30735	2.1×10^{-5}	0.97	16960	7.3×10^{-6}	0.41

3.4 Corrosion behavior study

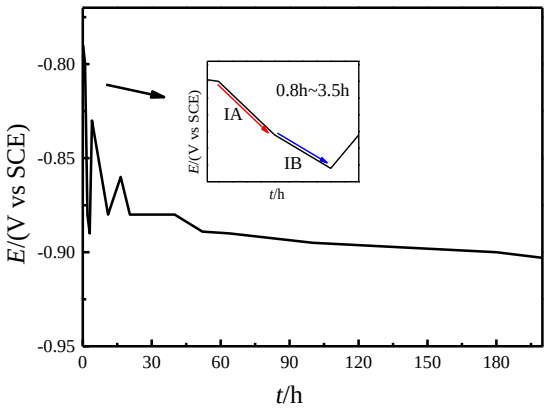

Figure 7. Open circuit potential curve of GPTMS-AIP-0.5 coating immersed in 5% NaCl for different time.

Figure7 shows the open-circuit potential curve of GPTMS-AIP-0.5 coating immersed in 5 wt% NaCl solution for different times. Fig. 9 shows the electrochemical impedance spectroscopy (EIS) of GPTMS-AIP-0.5 coating after immersion in 5 wt.% NaCl for different times, (a), (b), (c) displays the Nyquist curves and (d), (e), (f) displays Bode-Phase plots of the sample. An impedance spectrum is simulated using the equivalent electrical circuits as shown in Fig.8. CPEc, CPEox and CPEdl explain the semi-capacitor behavior of the absorbed ions in the coating, healing products and double layer, respectively. R_S, R_{PO}, Rox, Rt are used for the solution, coating, healing products, and charge transfer resistance, respectively.

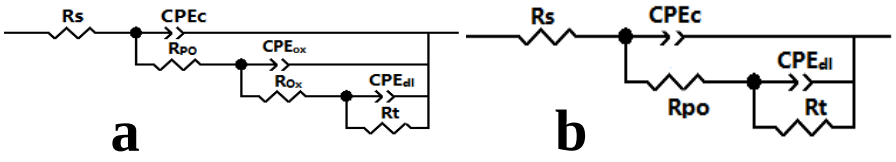

Figure 8. GPTMS-AIP-0.5 coating fitting circuit in different corrosion stages.

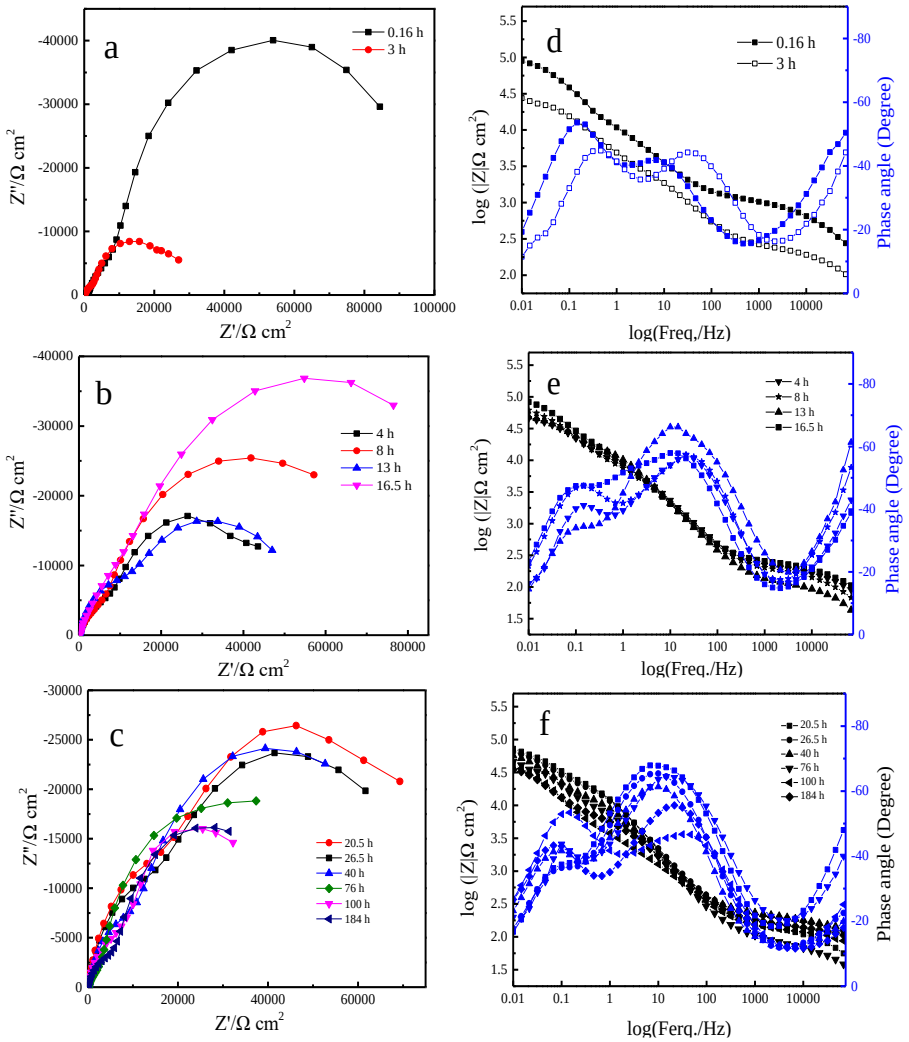

Figure 9. Electrochemical impedance spectroscopy of GPTMS-AIP-0.5 coating immersed in 5% NaCl for different time.

According to the variation trend of the open-circuit potential curve in Fig.7, the coating immersion process can be divided into three main stages:

The first stage was immersed from 0h to 3h, and the open circuit potential of the coating decreased continuously to -0.89 V. Depending on the rate of open-circuit potential decline, this stage can be divided into two subordinate stages: IA and IB. In the IA stage, the metal is protected by the shielding effect of the coating and the interaction between electrolyte and matrix is limited, which

prevents electrolyte solution from entering the inner layer, leading to a slow decline in the open-circuit potential of the coating. However, the rapid decrease of open-circuit potential in stage IB indicates that the corrosion resistance of coating is weakened during the immersion process, when electrolyte solution has begun to fully soak the coating and began to dissolve in the corrosive solution. Showed in Fig.9(a), during the first stage of immersion, the capacitive arc radii of the Nyquist diagram shows a rapid contraction and the impedance value at a low measured frequency decreases by nearly an order of magnitude, implying a decline of anticorrosion capability for the GPTMS-AIP-0.5 coating. According to the Bode-phase curve (Fig9(d)), the peak value of the phase moves to the high frequency region and moves down, the coating capacitance increases from 8.1×10^{-7}F/cm^2 to 1.9×10^{-5} F/cm^2, and the resistance of the coating decreases significantly, which are caused by electrolyte infiltration.

When the immersion time was from 3 h to 16.5 h, the coating corrosion entered the second stage. Open circuit potential rise to around -0.8 V, and stabilize in the range of -0.8 V to -0.9 V after repeated fluctuations. In the process of coating formation, organosilicon groups migrate to the outer surface of the coating, so that the coated rare earth ions will provide better corrosion resistance. At this stage, the rise of open circuit potential is due to the rupture of silane coating, which made the Ce^{3+} coated in the silane coating exposed in electrolyte solution. According to the research [25-27], the following reactions will occur when the coating is corroded:

Anodic reaction:

$$Al\text{-}3e^- \rightarrow Al^{3+}$$

Cathodic reaction:

$$O_2+2H_2O+4e^-\rightarrow OH^-$$

As the reaction progresses, pH of the anode decreases, while the pH of the cathode increases due to the reduction reaction of oxygen. Ce^{3+} released will have the following reaction:

$$Ce^{3+}+3OH^-\rightarrow Ce(OH)_3$$

$$4Ce^{3+}+O_2+4OH^-+2H_2O\rightarrow 4Ce(OH)_2{}^{2+}$$

$$Ce(OH)_2{}^{2+}+2OH^-\rightarrow CeO_2+2H_2O$$

After the reaction, $Ce(OH)_3$ and CeO_2 were generated near the cathode area, which filled pores and hindered the further occurrence of the reaction. Moreover, studies[28-30] have proved that Ce^{3+} has self-healing properties, which can repair corroded coatings. Compared with the last stage, the values of Rpo and Rox shown in table 3 were significantly increased because the generation of $Ce(OH)_3$ and CeO_2 prevented further corrosion and improved corrosion resistance of the coating. The conclusion is similar to J.Carneiro's research [24] and both proved that Ce-containing coatings confer active corrosion protection toward aluminum alloy. The equivalent circuit used to fit the impedance spectra of the first two corrosion stages is shown in Fig. 8(a). According to Fig.9(b), capacitive arc radii of the Nyquist diagram expanded instead of continuing the previous trend of contraction. Furthermore, the impedance value increased at low measured frequency and the value fluctuates repeatedly in a small range as well as the open-circuit potential. It proved that while the electrolyte solution constantly destroyed the coating structure, Ce^{3+} was continuously released and the defects of the coating were repaired. On the other hand, the significant increase of Rpo and Rox is due to the generation of $Ce(OH)_3$ and CeO_2, which prevented further corrosion and improved the corrosion resistance of the coating[31-32].

After the immersion time of 16.5 h, the coating entered the third stage of corrosion. Ce^{3+} within the coating is basically released completely and no longer plays a role in repairing the coating. As the immersion time increased, the coating structure was gradually destroyed, and its shielding effect on the electrolyte solution gradually weakened, the electrolyte solution can easily reach the metal surface at the same time. Therefore, the open circuit potential of the coating decreases steadily and slowly at this stage and finally drops to the open circuit potential of the substrate. It can be seen in Fig. 9(f), the impedance modulus of the coating decreases steadily and the peak value of the phase moves down, indicating a decline of anticorrosion capability for the coating[33]. The equivalent circuit used to fit the impedance spectra is shown in Fig. 8(b).

Table 3. Electrochemical impedance data of GPTMS-AIP-0.5 coating in the early stage of corrosion in 5% NaCl

t/h	R_{PO}	CPE_C		R_{OX}	CPE_{ox}		Rct	CPE_{dl}	
	($\Omega\cdot cm^2$)	$Y_0(F\cdot cm^{-2})$	n	($\Omega\cdot cm^2$)	$Y_0(F\cdot cm^{-2})$	n	($\Omega\cdot cm^2$)	$Y_0(F\cdot cm^{-2})$	n
0.16	1006	8.1×10^{-7}	0.69	14245	1.7×10^{-5}	0.73	90970	2.7×10^{-5}	0.92
3	1706	1.9×10^{-5}	0.75	3245	2.9×10^{-5}	0.65	20920	4×10^{-5}	0.93
8	4398	1.61×10^{-6}	0.74	15245	3.8×10^{-5}	0.58	35273	3.4×10^{-5}	0.65
13	19500	8.2×10^{-5}	0.79	23249	8.2×10^{-5}	0.88	86085	2.6×10^{-4}	0.45

Table 4. Electrochemical impedance data of GPTMS-AIP-0.5 coating in the middle and final stage of corrosion in 5% NaCl

t/h	R_{PO}	CPE_C		Rct	CPE_{dl}	
	($\Omega\cdot cm^2$)	$Y_0(F\cdot cm^{-2})$	n	($\Omega\cdot cm^2$)	$Y_0(F\cdot cm^{-2})$	n
20.5	34067	1.6×10^{-5}	0.81	44126	8.7×10^{-5}	0.95
26.5	28583	1.6×10^{-5}	0.8	42941	9.4×10^{-5}	0.94
40	19403	2.1×10^{-5}	0.78	51137	9.2×10^{-5}	0.9
52	12573	3.1×10^{-5}	0.73	44120	6.9×10^{-5}	0.93
76	14527	2.7×10^{-5}	0.78	32526	8.4×10^{-5}	0.94
100	5924	4.6×10^{-5}	0.67	52755	6.7×10^{-5}	0.88
184	8117	2.4×10^{-5}	0.75	40420	1.2×10^{-4}	0.84

4. CONCLUSION

Doping $Ce(NO_3)_3$ in the GPTMS-AIP coating can effectively improve corrosion resistance of the coating, and with the increase of the addition of $Ce(NO_3)_3$, the corrosion resistance of the coating

increased firstly after declining. When the concentration of $Ce(NO_3)_3$ is 0.5 g/L, corrosion resistance of the coating is the best, and the coating is homogeneous and flat without obvious defects.

According to the results of open-circuit potential and electrochemical impedance spectroscopy, the corrosion process of the coating in 5wt% NaCl solution can be divided into three stages: The first stage is the rupture of the outer silane film, which is characterized by the rapid decrease of the open circuit potential and impedance of the coating, and the corrosion resistance of the coating is obviously weakened; The second stage is the release of coated Ce^{3+} and the self-healing of the coating. In this stage, the open circuit potential rapidly rises from the low value and fluctuates in a certain range. This is because the generation of $Ce(OH)_3$ and CeO_2 filled the defects, prevented further corrosion and improved the corrosion resistance of the coating; In the third stage, the open circuit potential and impedance of the coating decreased slowly. The coating could not heal due to the complete consumption of the Ce^{3+}, shielding effect of the coating was gradually weakened in the soaking process, and the electrolyte solution could easily reach the base material.

References

1. M. Aamir, K. Giasin, M. Tolouei-Rad and A. Vafadar, *J. Mater. Res. Technol.*, 9 (2020) 12484.
2. A.Yabuki , Mod. Appl. Sci, 9 (2015) 7.
3. L. Shen, H. Chen, X. Che and Y. Wang, *Corros. Sci.*, 165 (2020) 108417.
4. J.Uruchurtu and J.L.Dawson, *Mater. Sci. Forum*, 8 (2012) 113.
5. B. Liu, X. Zhang, X. Zhou, T. Hashimoto and J. Wang, *Corros. Sci.*, 126 (2017) 265.
6. R. Ly, K.T. Hartwig and H. Castaneda, *Corros. Sci.*, 139 (2018) 47.
7. R.L. Twite and J.P. Bierwagen, *Prog. Org. Coat.*, 33 (1998) 91.
8. J. Qi, J. Swiatowska, P. Skeldon and P. Marcus, *J. Corros. Sci.*, 167 (2020) 108482.
9. X.V. Guardiola, J.P. Bonino, S. Duluard, B. Fori and C. Blanc, *Surf. Coat. Technol.*, 344 (2018) 276.
10. L.S. Kasten, J.T. Grant, N. Grebasch, N. Voevodin, F.E. Arnold and M.S. Donley, *Surf. Coat. Technol.*, 140 (2001) 11.
11. A.S. Hamdy, A.M. Beccaria and P. Traverso, *Surf. Interface Anal.*, 34 (2010) 171.
12. Q. Boyer, M.R.O. Vega, C.F. Malfitti, S. Duluard and F. Ansart, *Surf. Coat. Technol.*, 351 (2018) 115.
13. A.C. Bouali, M. Serdechnova, C. Blawert, J. Tedim, M.G.S. Ferreira and M.L. Zheludkevich, *Appli. Mater. Today.*, 21 (2020) 100857.
14. G. Bahlakeh, B. Ramezanzadeh and M. Ramezanzadeh, *J. Cleaner Prod..*, 210 (2019) 872.
15. V. Palanviel, Y. Huang and W.J.V. Ooij, *Prog. Org. Coat.*, 53 (2005) 153.
16. W. Tong, D. Xiong and H. Zhou, *Ceram. Int.*, 46 (2020) 1211.
17. C.A. Hernández-Barrios, J.A. Saavedra, S.L. Higuera, A.E. Coy and F. Viejo, *J. Surf. Interfaces*, 21 (2020) 100671.
18. V. Tsaryuk, V. Zolin, L. Puntus, V. Svachenko, J. Legendziewicz, J. Sokolnicki and R. Szostak, *J. Alloys Compd.*, 300 (2000) 184.
19. L.M. Palomino, Patrícia H.Suegama, I.V. Aoki, M.F. Montemor and Hercílio G. De Melo. *Corros. Sci.*, 81 (2009) 1238.
20. A.M. Cabral, W. Trabels, R. Serra, M.F. Montemor, M.L. Zheludkevich and M.G.S. Ferreira, *Corros. Sci.*, 48 (2006) 3740.
21. M.F. Montemor, W. Trabels, M. Zheludevich and M.G. S.Ferreira, *Prog. Org. Coat.*, 57 (2006) 67.

22. X. Pan, S. Wu, K. Xiao, S.Gao, L. Pei, R. Tian and X. Li, *Acta Metall. Sin.*, 49 (2013) 1113.
23. X.X. Sheng, W.X. Cai and L. Zhong, *Ind. Eng. Chem. Res.*, 31 (2016) 8576.
24. J. Carneiro, J. Tedim, S.C.M. Fernandes, C.S.R. Freire, A.J.D. Silvestre, A. Gandini, M.G.S. Ferreira and M.L. Zheludkevich, *Prog. Org. Coat.*, 75 (2012) 8.
25. H. Shi, E.H. Han and F. Liu, *Corros. Sci.*, 53 (2011) 2374.
26. J. Liu, D. Wang, L. Gao and D. Zhang, *Appl. Surf. Sci.*, 15 (2016) 369.
27. R.V. Lakshmi, S.T. Aruna, C. Anandan, P. Bera and S. Sampath, *Surf. Coat. Technol.*, 309 (2017) 363.
28. N.P. Tavandashti and S. Sanjabi, *Prog. Org. Coat.*, 69 (2010) 384.
29. R.V. Lakshmi, G. Yoganandan, K.T. Kavya and B.J. Basu, *Prog. Org. Coat.*, 76 (2013) 367.
30. Y. Castro, E. Ozmen and A. Duran, *Surf. Coat. Technol.*, 387 (2020) 125521.
31. S.V. Harb, A. Trentin, T.A.C. Souza, M. Magnani, S.H. Pulcinelli, C.V. Santilli and P. Hammer, *Chem. Eng. J.*, 383 (2020) 123219.
32. T.T. Thai, A.T. Trinh and M.G. Olivier, *Prog. Org. Coat.*, 138 (2020) 105428.
33. J.C. Martins, J.C.M. Neto, R.R. Passos and L.A. Pocrifka, *Solid State Ionics.*, 346 (2020) 115198.